Interfacial Flow of Simple Liquids on Polymer Brushes: Effect of Solvent Quality and Grafting Density

ARTICLE *in* MACROMOLECULES · JULY 2012

Impact Factor: 5.8 · DOI: 10.1021/ma300880y

3 AUTHORS, INCLUDING:

Thomas Lee
Massachusetts Institute of Technology
5 PUBLICATIONS **16** CITATIONS
SEE PROFILE

Shaun Hendy
University of Auckland
100 PUBLICATIONS **989** CITATIONS
SEE PROFILE

Macromolecules

Article

pubs.acs.org/Macromolecules

Interfacial Flow of Simple Liquids on Polymer Brushes: Effect of Solvent Quality and Grafting Density

Thomas Lee,[†] Shaun C. Hendy,*[,‡] and Chiara Neto*[,†]

[†]School of Chemistry, The University of Sydney, Sydney, NSW 2006, Australia

[‡]MacDiarmid Institute for Advanced Materials and Nanotechnology, Industrial Research Ltd., Lower Hutt, 5040, New Zealand, and School of Chemical and Physical Sciences, Victoria University of Wellington, Wellington 6140, New Zealand

ABSTRACT: We have used coarse-grained molecular dynamics simulations to study the boundary condition for the flow of a simple Newtonian liquid over a polymer brush. We investigated the dependence of the boundary condition on grafting density in good and poor solvents. In a good solvent the stagnation length for flow within the brush scales with the distance between chains D in accordance with the Alexander–de Gennes prediction for the brush height, as $D^{-2/3}$, while the height itself scales as D^{-2} due to a short chain length. In a poor solvent the polymer chains undergo constrained dewetting on the surface to form nanoscale patterns of polymer aggregates. When the boundary condition for flow at the polymer differs from that at the underlying substrate, patterns emerge in the flow, such that the liquid near the surface flows at different rates over the polymer and substrate. We have applied a simple model to relate the boundary condition at these patterned surfaces to the height and surface coverage of the polymer aggregates.

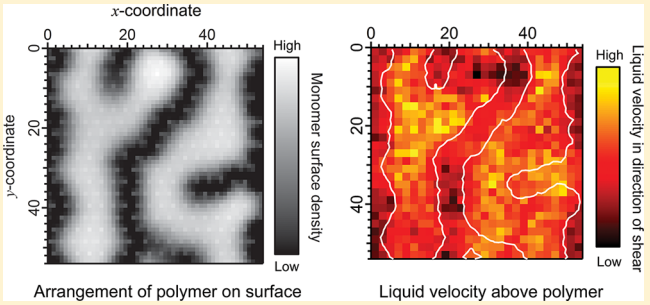

1. INTRODUCTION

The behavior of a simple liquid flowing at the interface with a solid has been a topic of debate for two centuries. Macroscopic hydrodynamic systems can be described using a no-slip boundary condition, which assumes the liquid has zero velocity at the solid–liquid interface. Advances in measurement techniques in recent decades have allowed the boundary condition to be probed on micro- and nanoscopic length scales. In many cases it has been shown that a slip boundary condition is more appropriate,[1] which indicates a nonzero liquid velocity at the interface. Even small deviations from the no-slip boundary condition are of critical importance when modeling the flow of liquids confined to microscopic geometries.

A great deal of work has been devoted toward determining the boundary condition of fluid flow at rigid surfaces.[1−4] Considerably less attention has been directed toward characterization of flow over surfaces composed of soft matter, such as polymer brushes. In addition to a vast number of possible chemical functionalities, soft matter surfaces have the potential to reversibly switch their properties and structure in reaction to changes in their environment, with potential application in responsive components for microfluidic devices.[5] The hydrodynamics of flows over soft surfaces are also of interest for their importance to the understanding of biological microfluidic systems, such as flow in blood vessels[6] and propulsion of microorganisms.[7] The compliance of a surface has the potential to significantly influence interaction with flows, with soft surfaces having been shown to significantly reduce drag in turbulent flows.[8]

The hydrodynamic boundary condition at a solid–liquid interface is defined in terms of the point at which the velocity profile of the fluid extrapolates linearly (in the case of Couette flow) to zero relative to the position of the interface. This is illustrated in Figure 1a for a rigid surface and in Figure 1b for a polymer brush in a good solvent. The boundary condition at a rigid surface is characterized by the slip length, b, with a slip length of zero corresponding to a no-slip boundary condition. Two metrics can be used to describe the boundary condition at a polymer brush. The stagnation length, l_s, is the distance from the substrate at which the flow appears to be completely inhibited by the brush based on a linear extrapolation of the velocity in the region above the brush. This is essentially a hydrodynamic measure of the height but will not necessarily coincide with the actual height. The penetration length, l_p, is the difference between the brush height and the stagnation length. It is the distance the flow appears to penetrate into the brush and is analogous with the slip length at a rigid substrate. The penetration length will be of interest when the difference between the hydrodynamic extent and physical extent of the brush is important.

There have been relatively few theoretical and computational attempts to describe the hydrodynamic penetration of flow into a polymer brush. The earliest attempt of which we are aware is by Milner.[9] To model the flow within a polymer brush with a parabolic monomer density profile, Milner employed the

Received: May 1, 2012
Revised: June 28, 2012
Published: July 20, 2012

   dx.doi.org/10.1021/ma300880y | *Macromolecules* 2012, 45, 6241−6252

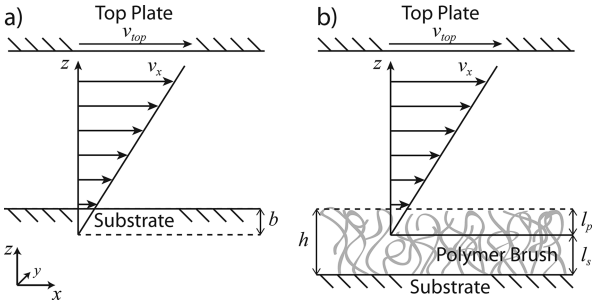

Figure 1. Schematic illustration of Couette slip flow over a rigid substrate (a) and over a polymer brush in a good solvent (b). Couette flow is imposed by moving the top bounding plate at a constant velocity, v_{top}, in the x-direction. This results in a linearly decreasing velocity from the top plate toward the brush. The slip length, b, at a rigid solid substrate is defined as the distance into the substrate at which the flow appears to linearly extrapolate to zero velocity. The stagnation length, l_s, is the distance from the substrate at which the flow appears to be completely inhibited by the brush, based on a linear extrapolation of the liquid velocity above the brush penetration length. The penetration length, l_p, is the difference between the brush height and stagnation length and is analogous to the slip length for a polymer brush.

Brinkman equation,[10] used to describe flows within polymer solutions with the same approach used to model to flow through a porous medium. When applied to a polymer solution, the effective pore size is taken as the mesh size, or correlation length, ξ, the characteristic length of the system, which is a function of the local monomer volume fraction. For a simple shear flow over a polymer brush, for which pressure terms are constant, the Brinkman equation reduces to

$$\frac{\partial^2 v}{\partial z^2} = \frac{v}{\xi^2(\phi)} \quad (1)$$

where v is the velocity of fluid flow, z is the distance from the solid substrate, and ϕ is the monomer volume fraction.[9] Recent studies suggest the Brinkman equation may not capture all aspects of flow, such as the details of the motion of the chains.[11]

There have been very few experimental attempts to characterize the penetration length at polymer brush surfaces. McLean et al.[12] used colloid probe atomic force microscopy (AFM), and results were in qualitative agreement with Milner's analysis. The majority of simulation and theoretical studies into flow over polymer brushes assume flow within the brush obeys the Brinkman equation, primarily in order to study the influence of solvent flow on the structure of the brush, including changes in height, and chain stretching and tilting.[13−17] Relatively few studies have explored the effect of the polymer brush on the boundary condition of the flow, and those that have either used free polymer as the solvent rather than a simple liquid[11,18] or were concerned specifically with highly confined nanopore geometries.[19−21] To study the boundary condition without making assumptions about the flow within the brush requires the use of an "explicit" solvent, in which the individual solvent atoms are explicitly included in the system. In contrast, the more common approach is to employ an "implicit" solvent in which a thermostat is used to mimic interactions between the polymer chains and a continuous background solvent at a constant temperature. The implicit solvent approach reduces computation time by greatly reducing the number of atoms that need to be simulated but makes restrictive assumptions about the flow within the brush. Implicit solvent studies have used the Brinkman equation to calculate the appropriate force to apply to the monomers in order to simulate the effects of flow.

The rapidly increasing availability of computational resources has made the simulation of an explicit solvent more and more practical. An explicit solvent allows us to avoid making assumptions about the flow within the polymer brush, allowing us to test the validity and limits of the Brinkman equation in this system, and explore finer details of the interaction between the flow and polymer chains. It has been shown, modeling the solvent as an explicit melt of polymers identical to the brush, that chains in the brush undergo a cyclic motion, moving in the direction of the flow near the edge of the brush, sweeping down below the reach of the flow, and finally being pulled back toward their equilibrium position.[11,18,22,23] Such dynamic behavior cannot be captured if an implicit solvent is used. While a number of recent studies have been reported in which the solvent is a melt of identical chains,[11,18,24,25] very rarely has a simple Lennard-Jones liquid been employed as a solvent.[21,26,27] This is an aspect in which we are particularly interested, as it mimics a simple Newtonian liquid.

Polymer brushes offer the possibility of reversibly switchable surfaces with the ability to respond to changes in their environment by changing their conformation.[5] When exposed to a good solvent, the brush is swollen with liquid and chains extend outward. In a poor solvent, however, the brush will collapse into a dense layer from which solvent is excluded.[28] Some polymers, when confined in a brush, allow this transition to be achieved by changes in temperature, pH, and ionic strength[29] or by application of an electric field.[30] This opens up the possibility of using polymer brushes as responsive microfluidic components. Clearly, the interaction of the polymer brush layer with a flowing liquid should depend strongly on solvent quality of the system. Such a change has been simulated for polymer brushes confined in a nanocapillary, demonstrating the potential for the brush to act as a valve, inhibiting flow through the capillary when swollen and opening it when the brush is collapsed by reducing solvent quality.[19,21,31,32]

The difference between brushes in good and poor solvent environments is not limited to changes in height and polymer volume fraction. When polymer brushes collapse in a poor solvent, the resulting layer will not in all cases be a flat continuous layer. At low to moderate grafting density a continuous layer of polymer is unstable.[33,34] This instability gives rise to a process referred to as constrained dewetting, which results in the polymer chains forming clumps on the surface, leaving some areas of the substrate exposed. The driving force behind this process is unfavorable intermolecular forces at the interface, as for the general dewetting of thin polymer films, with the added constraint of the covalent bonds to the surface. The morphology of this dewetted layer varies significantly with grafting density. As grafting density is increased, we pass through the regimes of pinned micelles,[35,36] flat-topped pancake micelles,[34] semicontinuous layers,[37] holey layers,[34] and finally a continuous film at high grafting density. Note that these aggregates, although commonly referred to as "micelles", are not true micelles, as the polymer chains composing the aggregate have no amphiphilic character, in contrast to micelles composed of surfactant molecules or block copolymers.

The flow at the interface may be influenced by the roughness that results from the heterogeneous nature of the dewetted

dx.doi.org/10.1021/ma300880y | Macromolecules 2012, 45, 6241−6252

polymer brush. But there is another factor that may also play a significant role. If the boundary condition for fluid flow at the substrate−liquid interface created upon dewetting differs from that at the polymer−liquid interface, a pattern of different boundary conditions at different locations on the surface will result. It would therefore be possible in principle to choose a substrate and polymer such that a surface with a pattern of slip and no-slip regions could be engineered as a novel component for microfluidic devices. Such components could include microfluidic mixers,[38] which could be turned on or off by switching the brush between a collapsed and swollen state.

In this work we have used course-grained molecular dynamics simulations to investigate the flow of an explicit solvent in the form of a simple Lennard-Jones liquid over a bead−spring polymer brush at various grafting densities in both good and poor solvent conditions. In the good solvent, we were particularly interested in the stagnation and penetration lengths and how these depend on the grafting density of the brush. In the poor solvent, we have focused on how varying the brush grafting density affects the morphology of the dewetted polymer layer and consequently the flow at the interface. In the poor solvent we have investigated the characteristics of flow over the pinned micelle, pancake micelle, and semicontinuous layer regimes in addition to a continuous layer at high grafting density. We compared the measured boundary condition with a simple model for slip over patterned surfaces based on a perturbative approach.

2. METHODS

We have used the freely available LAMMPS simulation package to run coarse-grained molecular dynamics simulations. We consider a polymer brush formed by fixing bead−spring polymers, composed of 19 monomers, by one end to a flat immobile substrate. A Lennard-Jones liquid is confined between the brush and a solid top plate, which is moved at a fixed velocity in order to induce Couette flow. The coordinate system is illustrated in Figure 1a. Periodic boundaries apply in the x and y dimensions. Solvent quality is controlled by adjusting the strength of the Lennard-Jones interaction between liquid and monomer atoms.

Interactions between any two nonbonded particles separated by a distance r were governed by a Lennard-Jones potential with a cutoff at $r_c = 2.5\sigma$.

$$E_{LJ} = 4\epsilon_{ij}[(\sigma/r)^{12} - (\sigma/r)^{6}]; \quad r < r_c \tag{2}$$

The σ parameter—approximately the size of the atoms—was the same for all atoms. The ϵ_{ij} parameter controls the depth of the potential well and strength of the attractive interaction between each pair of atoms i and j. All quantities will be expressed in terms of Lennard-Jones units for the interaction between two liquid atoms: distances in terms of σ, energy in terms of ϵ, and time in terms of $\tau = (m\sigma^2/\epsilon)^{1/2}$ where m is the atomic mass and is the same for all atoms. For interactions between monomers $\epsilon_{mm} = 1\epsilon$, identical to that for the liquid−liquid interaction. Between liquid and substrate atoms $\epsilon_{ls} = 1\epsilon$, but between monomer and substrate atoms $\epsilon_{ms} = 0.5\epsilon$ to reduce attraction between of the polymer chains to the substrate and reduce layering of the atoms against the substrate. The interaction between liquid and monomer atoms was varied to alter solvent quality. For a good solvent $\epsilon_{ml} = 1\epsilon$ such that liquid molecules are identical to the monomers, while for a poor solvent $\epsilon_{ml} = 0.25\epsilon$, leading to collapse of the brush due to the preference of monomers for each other rather than the liquid.

Interactions between bonded monomers were modeled with the commonly used finitely extensible nonlinear elastic (FENE) potential[39] with typical values for the parameters $k = 30\epsilon/\sigma^2$, $R_0 = 1.5\sigma$

$$E_{FENE} = -0.5KR_0^2 \ln\left[1 - \left(\frac{r}{R_0}\right)^2\right] + 4\epsilon\left[\left(\frac{\sigma}{r}\right)^{12} - \left(\frac{\sigma}{r}\right)^{6}\right] + \epsilon; \quad r < r_c \tag{3}$$

where the first term cuts off at R_0 and the second at $2^{1/6}\sigma$.

Polymer chains are grafted to the surface by an immobile monomer in the plane of the substrate atoms. Graft points are arranged in a rhombic lattice with lattice constant D, the chain separation, equal to the inverse square of the grafting density. The underlying substrate is composed of one layer of immobile atoms in a cubic lattice with lattice constant 1σ.

Chain separations between 2.01σ and 5.03σ are simulated. Relatively short chains (19 monomers long) are used in order to reduce computation time. Use of short chains means that scaling laws developed brushes composed of long chains may not apply,[40,41] and the exponential tail in the monomer density in the outer regions of the brush will be relatively large compared to the brush height.[42] Both these factors are addressed in our discussion of the results. The lateral dimensions of the substrate are adjusted in order to fit 64 chains for the good solvent. The number of liquid molecules in a simulation is 23 per σ^2 area of substrate. At $D = 2.01\sigma$, this corresponds to 6647 liquid atoms and at $D = 5.03\sigma$ to 14 375 atoms. For the poor solvent cases where constrained dewetting occurs, larger boxes are required such that the dimensions of the simulation are significantly larger than the length scale of the features. Lateral dimensions in this case are approximately $55\sigma \times 55\sigma$, varying slightly in order to ensure the lattice of polymer graft points is uninterrupted as periodic boundaries are crossed. For these systems between 50 000 and 60 000 liquid atoms are required.

The upper plate was composed of atoms in a square lattice lying with lattice constant σ. Upper plate atoms were allowed to move together in the y-direction. The y-component of the force on each atom in the upper plate was the average of the forces on these atoms due to interactions with the liquid, plus an additional constant downward force on the upper plate of $0.05m\sigma\tau^{-2}$ atom, thus applying a constant pressure to the system. The height of the simulation box varies somewhat both as a result of this and due to the differences of the structure of the atoms in the polymer brush region but is generally in the range 40σ to 50σ. Each system was subjected to five different shear rates in the range $0.004\tau^{-1}$−$0.010\tau^{-1}$, which corresponds to shear rates on the order of 10^9 s^{-1} in SI units, based on σ and ϵ values comparable to liquid water, $\sigma \approx 0.3$ nm and $\epsilon \approx 6.5 \times 10^2$ J mol^{-1}.[43]

A Langevin thermostat was applied in the y and z axes—perpendicular to the direction of shear. A dissipative force and a random force were applied to each particle in the y and z axes. The z-components of the thermostat forces are

$$F_z^{dissipative} = -\gamma v_z \tag{4}$$

$$F_z^{random} \sim \sqrt{\gamma T/dt} \tag{5}$$

dx.doi.org/10.1021/ma300880y | Macromolecules 2012, 45, 6241−6252

where v_z is the velocity in the z-axis, γ is the friction coefficient, T is the target temperature, and dt is the time-step. A uniform random number generator varied the sign and magnitude of F_z^{random}. The y-components of the thermostat forces, $F_y^{\text{dissipative}}$ and F_y^{random}, were calculated in the same manner as those in the z-component. No thermostat forces were applied in the x-axis, in which the shear is applied. The friction coefficient in these simulations was chosen as $5\tau^{-1}$. Although the Langevin thermostat does not conserve momentum, it has been shown that the characteristics of the steady state are similar to the momentum conserving dissipative particle dynamics (DPD) thermostat, providing the thermostat is switched off in the direction of shear.[26]

3. RESULTS

Polymer brushes were simulated under good and poor solvent conditions at a range of values of chain separation (i.e., the inverse square of the grafting density). In all our simulations the system was initially equilibrated without applying shear until polymer morphology stabilized, before imposing a Couette flow by moving the top plate at a fixed velocity in the x-direction. We will first discuss the behavior of these systems in good solvent conditions, followed by the poor solvent case.

3.1. Polymer Brushes in a Good Solvent. We have simulated the flow over polymer brushes in good solvent, for which the strength of the monomer−liquid interaction is equal to that of the monomer−monomer interaction, $\epsilon_{mm} = \epsilon_{ml}$. The schematic in Figure 2i illustrates the typical conformation of the

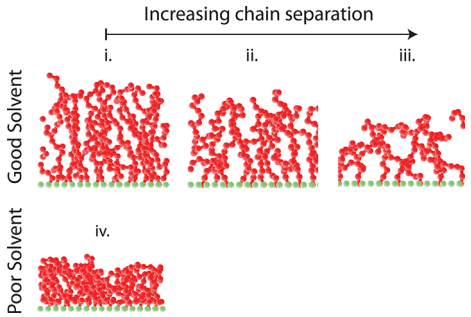

Figure 2. Schematics illustrating the qualitative features of polymer brushes in a good solvent at low (i), moderate (ii), and high (iii) chain separations and in a poor solvent at low chain separation (iv). Red spheres indicate monomers of the polymer, and pale green indicates substrate atoms. Solvent atoms are not displayed for clarity.

polymer brushes in a good solvent. Polymer chains in solution typically prefer a globular structure, but when contained in a brush, steric interactions between adjacent polymers force the chains to elongate, stretching away from the surface. The liquid penetrates significantly into the layer due to the high affinity of the monomers for the liquid.[28]

The structure of a brush depends strongly on the chain separation, D. When the chain separation is increased, as it is in Figures 2ii and 2iii compared to Figure 2i, the chains are not forced to elongate to the same degree and can acquire a more entropically favorable conformation. Since the chains are not packed as densely, more liquid may penetrate into the layer when chain separation is large. The mean radius of gyration of a single unbound chain surrounded by good solvent was measured in a separate simulation and found to be 2.19σ with a standard deviation of 0.39σ. At the largest chain separation studied, $D = 5.03\sigma$, the chains are near the high-density end of the mushroom regime—close enough for significant interaction, but not overlapping to a large extent. At the lowest chain separation, $D = 2.01\sigma$, there is a large degree of overlap between neighboring chains.

The structure of the brush changes significantly in a poor solvent, shown in Figure 2iv, for which $\epsilon_{ml} < \epsilon_{mm}$, such that the liquid−monomer interaction is weaker than the monomer−monomer interaction. The mean radius of gyration of a free chain in the poor solvent was 1.45σ with a standard deviation of 0.11σ. The volume occupied by the chain in poor solvent was therefore approximately half that occupied under good solvent conditions. The polymer brush in a poor solvent collapsed into a thin dense layer into which the liquid does not penetrate to any significant degree. The poor solvent case will be described in more detail later in this discussion.

The monomer density as a function of distance from the substrate $\phi(z)$ is shown in Figure 3. The monomer density at a

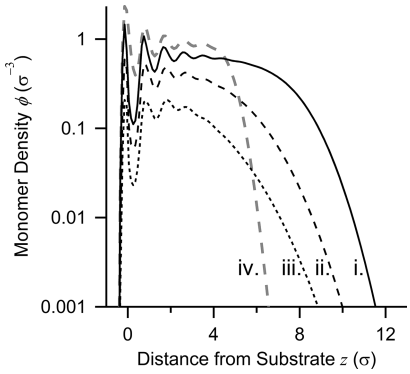

Figure 3. Monomer density as a function of distance from the substrate $\phi(z)$ on a log scale. Curves i, ii, and iii correspond to brushes in a good solvent at chain separations of 2.01σ, 3.02σ, and 5.03σ, respectively, and correspond to the similarly labeled schematics in Figure 2. Monomer density for a collapsed brush in a poor solvent at chain separations of 2.01σ is shown in (iv). The point $z = 0$ corresponds to the plane 1σ from the plane containing the center of the substrate molecules.

given distance from the substrate z was measured by averaging over time the number density of monomers in the region $z - 0.05\sigma < z < z + 0.05\sigma$. The point $z = 0$ corresponds to 1σ from the plane containing the center of the substrate molecules, which is approximately the edge of the repulsive region of the Lennard-Jones potential of the substrate particles. The rationale for this selection of zero is that at a substrate with a no-slip boundary condition and no polymer grafted to the surface the velocity of the solvent would be expected to be zero at the layer of liquid molecules adjacent to the substrate—positioned approximately 1σ from the center of the substrate particles. Curves i, ii, and iii correspond to a good solvent and chain separations $D = 2.01\sigma$, $D = 3.02\sigma$, and $D = 5.03\sigma$, respectively. Curve iv corresponds to a collapsed brush in a poor solvent with $D = 2.01\sigma$.

Ideal polymer brushes in the limit of long chains have a parabolic density profile, except for a small tail near the top of the brush with the theoretical form $\phi(z) \sim \exp[\text{constant}(z - h)^{3/2}]$, where h is the brush height.[44] Our polymers are considerably shorter than would be required to precisely follow the predicted density profile but do display the same general features of near-parabolic behavior plus a tail effect. Monomers near the base of the brush align with the substrate in a layering

effect, as seen in other simulations,[22] resulting in several peaks in the density in this region. The layering is not present in the outer regions of the brush, beyond approximately $z = 4\sigma$, and so should not have a significant impact on the interaction of the polymer with liquid flows. The average monomer density of the brush depends strongly on the chain separation, decreasing as chains are further from each other. Reduced monomer density within the brush allows a good solvent to more easily penetrate into the brush compared to brushes with lower chain separation.

The height of the polymer brush is conventionally taken as the first moment of the monomer density distribution, defined as $\langle z \rangle = \int z\phi(z)\, dz / \int \phi(z)\, dz$, which corresponds to the height as measured by ellipsometry.[45] Defining the height by $h = \langle z \rangle$ is not suitable for our purposes as a large fraction of monomers are located in the region $z > \langle z \rangle$. In the limit of a brush with step function monomer density, of the type employed by Alexander and de Gennes, the height h_{step} is exactly twice the first moment of the density. As a parabolic density profile provides a far better description of a polymer brush than a step function, we use the relationship derived by Milner et al. between the height of a step function brush and the equivalent parabolic brush, $h_{parabolic} = h_{step}/0.74$.[9,46] Thus, we use a definition the height of the brushes:

$$h_{para} \stackrel{def}{=} 2z/0.74 \tag{6}$$

which allows comparison with scaling laws for the first moment while also providing a reasonable approximation for the top of the brush.

However, this definition of height fails to take into account the small region in the tail of the brush extending beyond this point, which we will see later in this article is an important factor when describing the hydrodynamic penetration into the brush. We have used an approximate definition of the height including the tail region, h_{tail}, as the value of z at which the density falls to $0.001\sigma^{-3}$, such that the vast majority of the monomers are located within the range $0 < z < h_{tail}$. The disadvantage of this definition is that it does not allow comparison with the wider literature, which tends to measure height in terms of either the first moment of the density or the z-component of the radius of gyration. We will refer to both h_{tail} and h_{para} when discussing brushes in a good solvent, the difference between them can be seen in Figure 5 in which both are labelled. When describing the collapsed brush in a poor solvent, the distinction is less critical due to the more rapid decrease in density near the top of the brush, and in this case we describe the height only in terms of h_{tail}.

The relationship between chain separation and brush height, h_{para} and h_{tail}, under good solvent conditions is shown in Figure 4. The decrease in height with increasing chain separation is a result of reduced steric interactions between neighboring chains, allowing individual chains to adopt more entropically favorable conformations. We were able to fit both h_{para} and h_{tail} to a scaling law with the form

$$h = c_1 D^{\lambda} + c_2 \tag{7}$$

For h_{para} we obtained values $\lambda = -2.1 \pm 0.1$, $c_1 = 15.9 \pm 0.9$, and $c_2 = 6.42 \pm 0.07\sigma$ (errors are standard deviations), and this fit is plotted in Figure 4. This is consistent with other studies which have found that the height of polymer brushes composed of short chains with fewer than 50 monomers in a good solvent scales linearly with grafting density, or D^{-2}.[40,41] Much longer

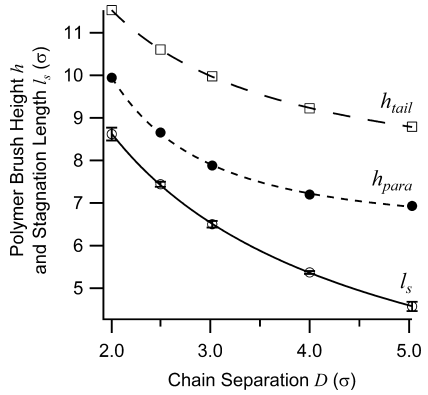

Figure 4. Height based on the first moment of the density h_{para} (●) and on the extent of the tail region h_{tail} (□) and the stagnation length (○) of polymer brushes in a good solvent as a function of chain separation. Uncertainties in the height are less than the size of the markers. The height h_{para} and h_{tail} were fitted to $h = c_1 D^{\lambda} + c_2$, with best fits when $\lambda = -2.1 \pm 0.1$ for h_{para} (short dashed line) and when $\lambda = -1.11 \pm 0.04$ for h_{tail} (long dashed line). Stagnation length is an average of measurements at five different shear rates and is fitted to $l_s = AD^{\lambda}$, with best fit when $\lambda = -0.691 \pm 0.003$ (solid line).

chains are required in order to observe the $h_{para} \sim D^{-2/3}$ relationship predicted by Alexander[47] and de Gennes[48] scaling analysis.

For h_{tail} the best fit was found when $\lambda = -1.11 \pm 0.04$, $c_1 = 9.33 \pm 0.08$, and $c_2 = 8.24 \pm 0.09\sigma$. Thus, h_{tail} does not follow the same scaling as h_{para}. The exponent λ and the c_1 coefficient are significantly lower in magnitude than fitted for h_{para}, indicating that h_{tail} is less sensitive to changes in chain separation.

Once the system equilibrated, Couette flow was initiated over the polymer brush by moving the top plate of the system at a constant velocity in the positive x-direction. The monomer density profile did not change significantly in response to the flow, which is consistent with previous theoretical,[17] computational,[14,15] and experimental[49,50] studies. Velocity of the liquid in the x-direction v_x as a function of distance from the substrate z was averaged over time, in the same manner as the monomer density, described earlier. The velocity above a polymer brush in a good solvent, decreases linearly as we approach the brush surface from large to small z, as shown in Figure 5. At a distance from the brush surface comparable to the brush height, the gradient of the velocity begins to decrease. The velocity decays as we approch the surface until a point within the brush is reached at which the flow is completely inhibited. This velocity profile is in qualitiative agreement with previous computational and theoretical studies of similar systems.[9,11,16,22]

We fitted a straight line to the velocity in the region $h_{tail} + 4\sigma < z < h_{tail} + 14\sigma$, which avoids perturbations in velocity due to the polymer brush. The shear rate was determined from the gradient of the fit. We also identified the value of z at which the fit extrapolates to zero velocity—the stagnation length l_s. We used the linear fit to define the stagnation length, rather than the point at which the actual velocity decays to zero, to reflect the practice commonly used in experimental studies.[4] The dependence of the stagnation length on the shear rate for the range of shear rates studied was negligible, and so the stagnation lengths we report are the mean of the stagnation lengths at the various shear rates and errors the 95% confidence interval of the mean. For the polymer brush shown in Figure 5,

dx.doi.org/10.1021/ma300880y | Macromolecules 2012, 45, 6241−6252

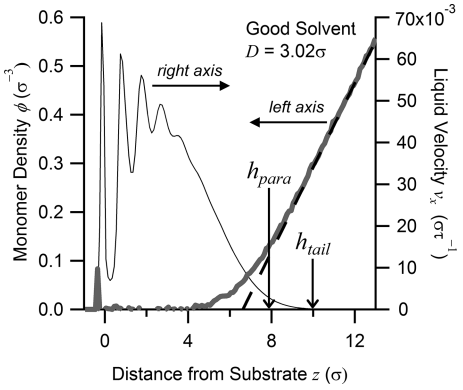

Figure 5. The x-component of the liquid velocity as a function of distance from the substrate $v_x(z)$ (i.e., the component of the velocity in the direction that the system is sheared) of a liquid flowing over a polymer brush in a good solvent (gray thick line, right axis), with a chain separation $D = 3.02\sigma$. A straight line has been fitted to the liquid velocity in the region far from the brush (dashed line). The monomer density as a function of z is also shown (thin line, left axis), and the heights h_{para} and h_{tail} are indicated by the arrows.

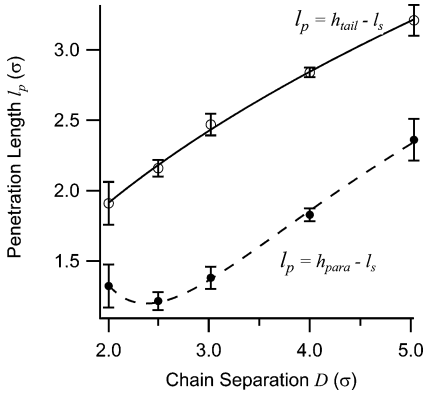

Figure 6. Penetration length l_p (●) of flow into the polymer brush in a good solvent as a function of chain separation D. Errors indicated are the 95% confidence interval based on measurements at five different shear rates. The dashed line is a fit to eq 8. The open circles (○) are the penetration length obtained when h_{tail} is used as the height, thus taking into account the tail in the monomer density. The fit in this case is to a simple scaling law $l_s = AD^{\lambda}$, with $\lambda = 0.40 \pm 0.01$.

the heights h_{para} and h_{tail} were 7.9σ and 10.0σ, respectively, and the stagnation length $7.50\sigma \pm 0.08\sigma$.

The stagnation length decreased with increasing chain separation, as shown in Figure 4, just as the height did. The stagnation length was well fitted by a scaling law, $l_s = AD^{\lambda}$, with best fit $A = 13.98 \pm 0.05$ and $\lambda = -0.691 \pm 0.003$ (the errors are standard deviations of the fitted constants). This relationship is strikingly similar to the predicted relationship between brush height and chain separation $h \sim D^{(\nu-1)/\nu}$,[51] where ν is the excluded volume exponent, which for a polymer in a good solvent is close to 3/5. If we assume that the stagnation length obeys the same power law as the height, our result $\lambda = -0.691 \pm 0.003$ corresponds to an excluded volume exponent $\nu = 0.591 \pm 0.003$, very close to the expected value for a good solvent. This result is particularly interesting in light of the fact that the first moment of the brush density, on which we base our calculation of brush height, scales as D^{-2} rather than $D^{-2/3}$.

The difference between the stagnation length and the height of the brush h is referred to as the penetration length l_p and is the extent to which the flow appears to penetrate into the polymer brush,[9] as illustrated in Figure 1b. This is analogous to the slip length at rigid substrates, which identifies the distance into the substrate at which the extrapolated velocity appears to reach zero. A nonzero slip length indicates that the fluid at the interface has a nonzero velocity. The penetration length of Couette flow of a good solvent into polymer brushes is shown in Figure 6 for a range of chain separations. At high to moderate values of D, the penetration length increases with increasing chain separation. This is expected, as polymer chains are less rigid and have more freedom to move with the flowing liquid when further apart. There appears to be a minimum in the penetration length at a value of D near 2.5σ.

As the height and stagnation length both appear to be governed by scaling laws with exponents consistent with -2 and $-2/3$, respectively, the penetration length can be modeled as the difference between these scaling laws. The fit to the filled circles in Figure 6 is to the function

$$l_p = C_h D^{-2} - C_s D^{-2/3} + C \qquad (8)$$

with best fit obtained for coefficients $C_h = 16.3 \pm 0.9$, $C_s = 15.3 \pm 0.7$, and $C = 6.9\sigma \pm 0.2\sigma$. The cause of the minimum penetration length at $D = 2.4\sigma$ is the fact that the influence of the positive $C_h D^{-2}$ term dominates over the negative $-C_s D^{-2/3}$ term as D approaches zero.

An effect that can only be observed if an explicit solvent is used is the cyclic motion of the polymer chains in the outer region of the brush. Several studies of flow of a polymer melt over a brush of identical chains have observed that near the top of the brush the chains have a net momentum in the direction of the flow, while some distance into the brush the chains move against the flow back toward their equilibrium position.[11,18,23] We have observed the same behavior, as shown in Figure 7

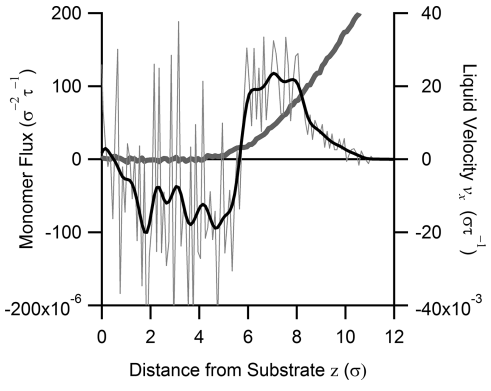

Figure 7. Monomer flux in the direction of shear (thin gray line), calculated as monomer density multiplied by monomer velocity in the x-direction, as a function of distance from the substrate, for a polymer brush in a good solvent with a chain separation $D = 3.02\sigma$. A binomial smoothing algorithm has been applied in order to reduce noise (black line). The velocity of the liquid in the x-direction in the direction of shear is also shown (thick gray curve).

which shows the monomer flux (density multiplied by velocity) as a function of distance from the substrate. Near the top of the brush the monomer flux is positive, i.e., in the direction of liquid flow. There is a point at which the direction of monomer flow reverses, which occurs quite suddenly. Between this point and the substrate, monomer velocity is relatively low, resulting

dx.doi.org/10.1021/ma300880y | Macromolecules 2012, 45, 6241−6252

in a low signal-to-noise ratio. The underlying trend can be observed by applying a binomial smoothing to the data which shows a clear trend for negative velocity in this region. The velocity of the liquid is also shown in Figure 7.

The distance from the substrate at which the reversal in monomer flow direction occurs, which we will refer to as the flow reversal length, is shown in Figure 8, along with the

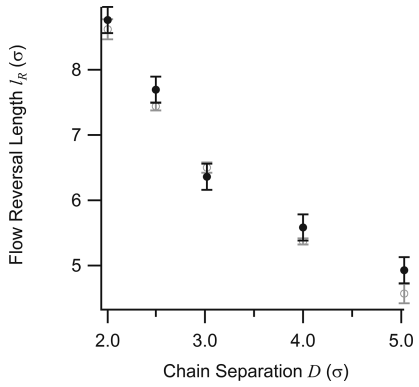

Figure 8. Flow reversal length (●), or the distance into the polymer brush at which the direction of monomer flow changes sign, as a function of chain separation. Stagnation length is also shown (○) for comparison.

stagnation length in gray for comparison. Flow reversal length is generally similar to the stagnation length; however, the flow reversal length has a larger error, and so we have not attempted to fit this data to a function.

3.2. Collapsed Polymer Brush in a Poor Solvent. In the following we turn our attention to polymer brushes in a poor solvent. A poor solvent was simulated by reducing the strength of the interaction between monomer and liquid atoms such that $\epsilon_{ml} = \epsilon_{mm}/4$. Reducing the solvent quality resulted in the expulsion of the solvent from the brush, creating a layer with a greater density and reduced height, as can been seen from the plot of density versus distance from the substrate in Figure 3iv, alongside the same brush in a good solvent in Figure 3i. The monomer density is relatively constant within the brush layer as we move away from the substrate, until a point is reached—approximately $z = 5\sigma$ in Figure 3iv—at which the density decreases sharply.

The collapsed brush in Figure 3iv had a small chain separation of 2.01σ. Under these conditions a continuous, uniform polymer layer is formed. At high and moderate chain separation, constrained dewetting took place, which resulted in the breakup of the collapsed brush into localized aggregates, separated by regions of exposed substrate. Examples of the structures formed under these conditions can be seen in Figure 9, which shows the variations in the monomer surface density over the substrate. These structures occurred as a result of the competition between the polymer's drive to minimize contact with the poor solvent and the penalty imposed on aggregation by the tethered nature of the chains.[34] At large chain separation, such as in Figure 9a,b, features commonly referred to as pinned micelles were formed.[34] These features have also been referred to as "octopus" micelles[52] due to the appearance of the chains stretching from the micelle to their point of attachment located outside the aggregate, as can be seen in Figure 9a in which the vast majority of the chains have a graft point that is not located directly underneath a micelle.

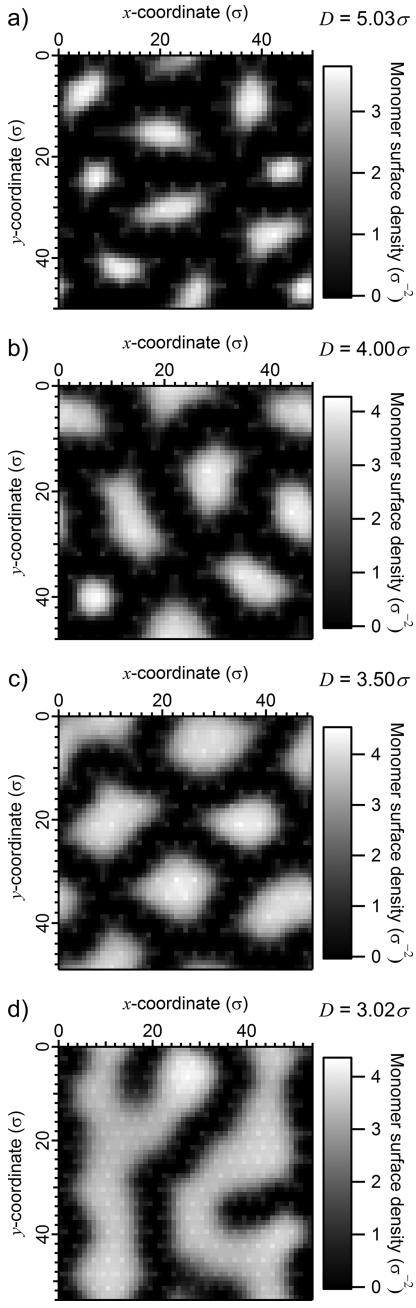

Figure 9. Surface density of grafted polymer layers in poor solvent conditions at chain separations of 5.03σ (a), 4.0σ (b), 3.5σ (c), and 3.02σ (d). Constrained dewetting resulted in the formation of pinned micelles observed in (a), (b), and (c). Below a certain chain separation, micelles joined together to form semicontinuous networks as in (d).

The size of the micelles increased with decreasing chain separation, and the number of distinct micelles in a given area was reduced. This is clearly seen by comparing Figure 9c with $D = 3.5\sigma$ and Figure 9a with $D = 5.03\sigma$. At $D = 3.5\sigma$ and 4.0σ pancake micelles[34] with flattened tops were formed. At a chain separation of 3.02σ, adjacent micelles joined together to form semicontinuous networks such as the one shown in Figure 9d. We see clearly in Figure 10 that the surface coverage of the polymer increases as the chain separation is decreased, reaching 100% coverage by $D = 2.01\sigma$. The dimensions of the features

dx.doi.org/10.1021/ma300880y | Macromolecules 2012, 45, 6241−6252

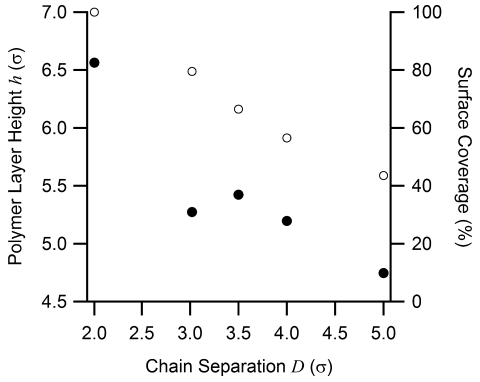

Figure 10. Height (●) and surface coverage (○) of the collapsed polymer brush in a poor solvent as a function of chain separation. Height is defined in the same manner as h_{tail} in a good solvent, as the distance from the substrate at which the monomer density reaches $0.001\sigma^{-3}$.

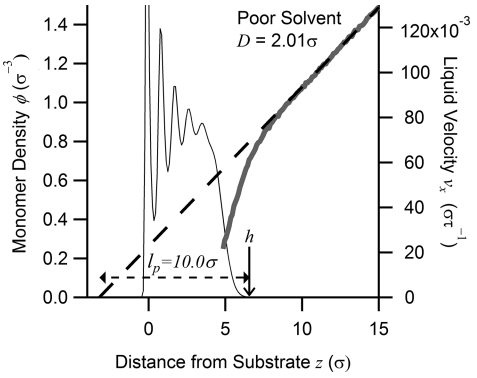

Figure 11. The x-component of the liquid velocity, $v_x(z)$, as a function of distance from the substrate (i.e., the component of the velocity in the direction the system is sheared) of a liquid flowing over a collapsed polymer brush in a poor solvent (thick line, right axis), with a chain separation $D = 2.01\sigma$. A straight line has been fitted to the liquid velocity in the linear region above brush (dashed line). The monomer density as a function of z is also shown (thin line, left axis), and the height of the brush, h, is indicated by the arrow. The velocity has not been plotted in the region close to the substrate where the number of liquid atoms present is negligible.

vary from micelles approximately 5σ across when $D = 5.03\sigma$ to extended aggregates around 10σ wide when $D = 2.01\sigma$.

The details of the pattern depend in part on the initial conditions of the simulations. We have generated different patterns by using different random number seed values to generate different initial monomer velocities at the beginning of the simulations. While the exact morphology of the patterns varied with different initial conditions, the general features for a given value of chain separation were the same. Connections between micelles occasionally broke and formed as the simulation progressed, even after long equilibration times, which in some cases resulted in slightly different patterns at different stages of the simulation.

The height of the grafted polymer layers in the poor solvent is shown in Figure 10. The height has been defined in the same manner as h_{tail} for the good solvent, as the distance from the substrate at which the average density throughout the simulation box is equal to $0.001\sigma^{-3}$. The height was greatest at the smallest chain separation studied, but interestingly, the height did not decrease monotonically with increasing chain separation. As chain separation increased from $D = 3.02\sigma$ to $D = 3.5\sigma$ the height increased by a relatively small but significant amount. This is likely due to the fact that the formation of the semicontinuous layer at $D = 3.02\sigma$ allowed the chains to spread laterally to a greater degree than in the more localized pinned micelles which formed at $D = 3.5\sigma$, in which the chains are too far apart to stretch between micelles and so must pile up. The height decreased monotonically as the chain separation was increased from $D = 3.5\sigma$ to $D = 5.03\sigma$. As micelles get smaller, chains must extend some distance along the surface to take part in the formation of a micelle. Fewer monomers are therefore present in the bulk of the micelle, resulting in a reduction in height. These trends are in qualitative agreement with previous studies.[34]

The patterns have interesting consequence for the flow over the collapsed polymer brush. They lead to not only a variation in height across the surface but also a variation in hydrodynamic boundary condition, the consequences of which will be discussed later.

3.3. Flow over Collapsed Polymer Brushes. As for the good solvent case, Couette flow was driven over the surface by moving the top plate after the system was equilibrated. Qualitatively different behavior was observed in the poor solvent compared with the good solvent, as shown in Figure 11 for a collapsed brush with $D = 2.01\sigma$, which formed a continuous and uniform layer. Again the velocity in the x-direction decreased linearly as the distance from the substrate decreased. As the top of the collapsed brush is approached, the gradient of the liquid velocity increases rapidly and the velocity reaches zero at a value of z significantly greater than the point at which the linear fit to the velocity reaches zero. The height in this case is 6.56σ, and the apparent penetration length is $10.0\sigma \pm 0.1\sigma$. As there is no significant infiltration of the liquid into the collapsed polymer brush, clearly there is not actually any liquid flowing as far into the polymer as the penetration length. In this case the penetration length coincides with a slip length. The large slip length is a result of the reduced strength of the interaction between liquid and monomer.

The constrained dewetting at large and intermediate chain separation opened an interesting scenario of a patterned boundary condition. In our simulations the interaction between the liquid and the substrate was chosen such that a no-slip boundary condition applied, while the slip length on the collapsed brush, as seen in Figure 11, was on the order of 10σ. In Figure 12, the effect of the variations in boundary condition on the flow of the solvent is clearly illustrated. The black–red–yellow colors in the figure indicate the velocity of the liquid in the direction of shear immediately above the polymer layers. The white lines in the figure show the outline of the polymer aggregates. The slip boundary condition over the polymer aggregates results in a significantly greater liquid velocity over these regions in both (a) and (b) (which correspond to the same systems as surface density images shown in Figures 9b and 9d). Similar correlations are observed for all chain separations studied.

A secondary effect can be seen, particularly in Figure 12a, in which the velocity over the no-slip regions seems to depend to some degree on the arrangement of the polymer aggregates nearby. For a given point $(x, y) = (a, b)$ over the bare substrate, when polymer aggregates are located immediately in front and behind the flow, at $x > a$ and $x < a$, the liquid velocity experiences greater than average slowdown. Conversely, if polymer aggregates are located to the left and right of the flow,

dx.doi.org/10.1021/ma300880y | Macromolecules 2012, 45, 6241–6252

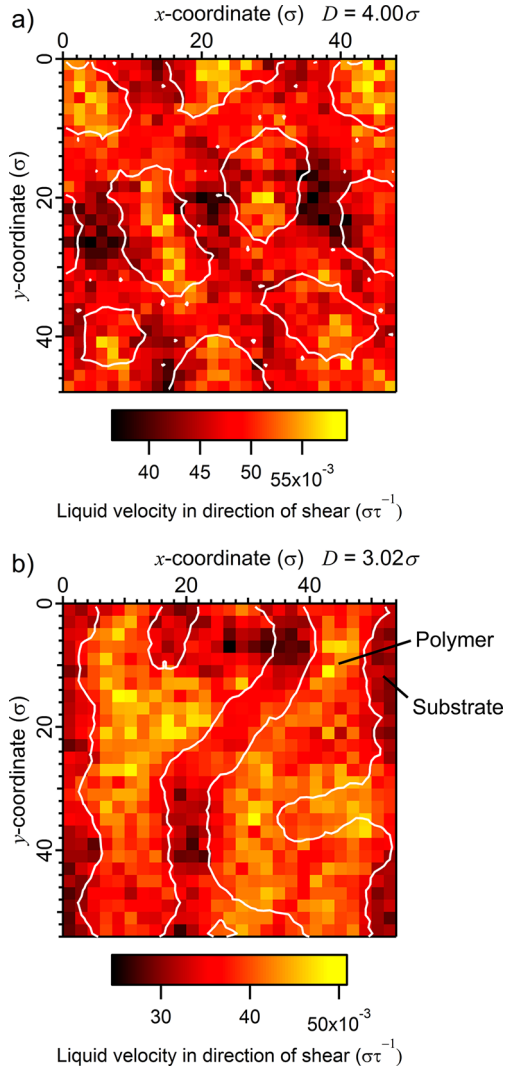

Figure 12. The x-component of liquid velocity immediately above the polymer layer in poor solvent at chain separations of 3.02σ and 4.0σ. Colors indicate liquid velocity in the direction of the shear. The morphology of the patterns in (a) and (b) can be seen in Figures 9b and 9d, respectively. White lines are contours indicating the points where the monomer surface density is equal to one, i.e., approximately the edges of the polymer aggregates. These systems correspond to the surface density images shown in Figures 9b and 9d, respectively.

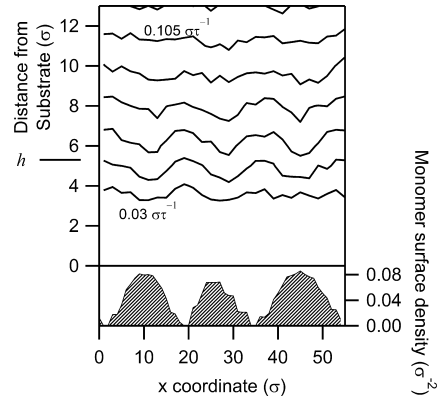

Figure 13. Velocity of the liquid above the pattered substrate correlates with the location of the polymer aggregates. The contours represent lines of constant velocity in increments of $0.15\sigma\tau^{-1}$. Far from the surface these lines are relatively flat, while closer to the top of the polymer layer fluctuations are observed which correlate with changes in the monomer surface density, shown on the right axis.

to the length scale of the pattern features, which are also on the order of 10σ in this case.

3.4. Average Boundary Condition at Collapsed Polymer Brushes. An example average velocity profile of the liquid above a semicontinuous polymer layer in a poor solvent is shown in Figure 14. This corresponds to the surface

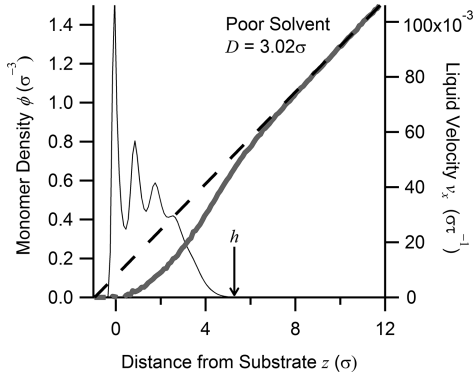

Figure 14. The x-component of the velocity, v_x, of a liquid flowing over a grafted polymer layer in a poor solvent (thick line), with a chain separation $D = 3.02\sigma$. A straight line has been fitted to the liquid velocity in the region far from the brush (dashed line). The density profile of the polymer is also shown (thin line).

or $y < b$ and $y > b$, the velocity in the x-direction appears to get a boost. In Figure 12b the effect is less obvious, but we can see in the region over the exposed substrate around the coordinate $(x, y) = (30, 20)$ that the velocity is higher than in other no slip regions. Similar behavior is observed in the regions around coordinates (40, 36) and (38, 50). These areas of the surface are the only areas for which the regions immediately left $(y < b)$ and right $(y > b)$ of the flow are covered with polymer, consistent with our observation in regard to Figure 12a.

The correlations between liquid velocity and polymer surface density is also illustrated in Figure 13, which shows velocity contours above the polymer layer for a cross section in the x–z plane of the system shown in Figure 12b at $y = 0$. The velocity varies significantly across the surface up to approximately $z = 10\sigma$, at which the flow appears to average out. We expect the distance over which the correlations dissipate to be comparable shown in Figure 9c. In the region where z is less than the height of the polymer layer, the liquid velocity corresponds to liquid flowing between the gaps of the polymer aggregates, rather than flowing within the polymer brush, as was the case in the good solvent.

A feature that is characteristic of the velocity profiles at these surfaces—and not observed by us on any surface we have studied without a pattern in boundary condition—is the inflection point which occurs in the outer regions of the polymer layer, as visible in Figure 14. At this inflection point, when approaching the surface from large z, $v_x(z)$ transitions from positive curvature (concave down) to negative curvature (concave up). By comparison, the velocity behavior in Figure 11 (poor solvent) and Figure 5 (good solvent) shows negative and positive curvature, respectively, at the interface between polymer and bulk liquid. This behavior can be explained by the

dx.doi.org/10.1021/ma300880y | Macromolecules 2012, 45, 6241–6252

fact that the velocity profile in Figure 14 is approximately a superposition of the profile over the no-slip regions of the exposed substrate—for which the velocity profile had a positive curvature near the substrate—and the slip regions of the polymer layer—for which the velocity profile had a negative curvature at the top of the polymer layer.

The boundary condition has been expressed as a penetration length in Figure 15. The apparent penetration is influenced by

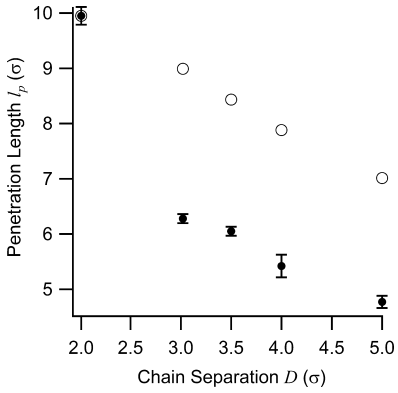

Figure 15. Penetration length (●) as a function of chain separation for a polymer layer in a poor solvent. An attempt has been made to predict the penetration length from the height and surface coverage of the polymer based on the model in eq 10 (○).

both the slip of the liquid on the polymer covered regions and the penetration of the flow into the regions between the polymer aggregates. This could equivalently be referred to as an effective slip length, where the no-slip scenario is defined as the case where the liquid velocity extrapolates to zero at the top of the polymer aggregates.

The penetration length decreased monotonically as the chains were moved further apart. The decrease in the penetration length between $D = 2.01\sigma$ and $D = 3.02\sigma$ is very rapid compared to the more gradual decrease between $D = 3.02\sigma$ and $D = 5.03\sigma$. This suggests that the increased exposure of the no-slip substrate is a dominant factor in determining the effective boundary condition.

We have used a perturbative approach to calculate a first order approximation of the penetration length, based on that employed by Hendy and Lund[53] to describe the effective boundary condition at flat surfaces with a patterned slip length. When the slip length at any point on the surface is less than the length scale of the pattern, the effective slip length can be approximated as $b_{eff} = \langle b(x,y)\rangle$, where $b(x,y)$ is the local slip length at a given point on the surface.[53] In order to take into account the surface roughness in our system, we modify the local slip length by subtracting the height:

$$b_{eff} = <b(x, y) - h(x, y)> \quad (9)$$

where the angle brackets indicate the average value of the function over the surface.

To predict the penetration length, we approximate the polymer covered regions as being a constant height h above the uncovered substrate, where h is the height plotted in Figure 10. We have assumed the slip on the polymer regions is equal to the penetration length for the case when a continuous layer is formed at $D = 2.01\sigma$, which is approximately 10σ. The slip length on the exposed substrate is zero. The predicted penetration length is therefore $l_p = \beta b_{polymer} + (1 - \beta)h$, where β is the area fraction of the surface covered by polymer, shown in Figure 10. This rearranges to

$$l_p = \beta(b_{polymer} - h) + h \quad (10)$$

As shown in Figure 15, the model successfully predicts the general trend for the penetration length to decrease monotonically with chain separation. The magnitude of the penetration length is overestimated due to the fact that the slip length is comparable to the pattern length scale.[53] The accuracy of the model might be improved by including second-order terms.

4. DISCUSSION

4.1. Brushes in a Good Solvent. We have analyzed the boundary conditions at polymer brush surfaces and investigated the dependence of these boundary conditions on solvent quality and grafting density. In the good solvent our polymers have shown the expected equilibrium behavior. Monomer density profiles in Figure 3 qualitatively agreed with the expected parabolic form, with a tail in the outer limits of the brush.[48] As chain separation was reduced, brush height decreased, as shown in Figure 4. The height based on a parabolic density profile approximation h_{para}—proportional to the first moment of the monomer density—varied in proportion with the inverse square of the chain separation, D^{-2} (equivalent to the grafting density), as is typical for short polymer chains in both simulations[40] and experiment.[41,54] However the stagnation length, effectively a hydrodynamic measure of brush height, scaled in proportion with $D^{-2/3}$, as shown in Figure 4, consistent with Alexander and de Gennes' prediction for much longer brushes.[47] This suggests there is a significant discrepancy between hydrodynamic measurements of the brush height, which would return l_s, and those which probe the density profile more directly, such as measurements based on interaction with electromagnetic radiation or neutrons, which would be reported in terms of $\langle z\rangle$, proportional to h_{para}.

The penetration length of the flow can be expressed as the difference between the brush height and stagnation length, $l_p = h - l_s$. Assuming $h = h_{para}$, the penetration length should obey eq 8. This expression has been fitted to the filled circles in Figure 6. The fact that the height term h_{para} scales as D^{-2}, while the stagnation length term, l_s, scales only as $D^{-2/3}$, results in a penetration length that increases with increasing D at moderate to large chain separations but decreases with increasing D when D is small. The minimum in the fitted curve occurs at $D = 2.4\sigma$. In other words, the presence of the minimum is due to the fact that l_p depends on the chain separation as the difference between the two scaling laws governing its components.

The presence of a minimum in penetration length at small D contradicts the expectation that penetration length is determined largely by the correlation length of the brush, ξ, which should increase as chain separation increases. Therefore, one would expect the penetration length to increase monotonically as chain separation increases. This discrepancy appears to arise because defining the height as h_{para} neglects the influence of the tail of the monomer density in the outer region of the brush. We can test this by defining the height as $h = h_{tail}$ which is sensitive to the presence of the tail. This measure of height scales approximately as $h_{tail} \sim D^{-1.1}$, as seen in Figure 4. Because h_{tail} is less sensitive to D than h_{para}, the penetration length calculated as $l_p = h_{tail} - l_s$, shown in Figure 6, increases monotonically with D for all D greater than 1σ, the smallest

dx.doi.org/10.1021/ma300880y | Macromolecules 2012, 45, 6241−6252

physically reasonable value of D. Calculated in this manner, the penetration length approximately resembles a scaling law $l_p \sim D^{0.40\pm0.01}$. As the gradient dl_p/dD varies only slowly over the range of chain separations studied, the penetration length is nearly linear with D, as predicted by application of the Brinkman equation (eq 1) to a step-profile brush. This suggests that a reasonable first-order approximation of the scaling of the penetration length can be obtained from Brinkman equation, which could be employed as a guiding principle in experiments of how boundary conditions change with chain separation.

The above analysis should apply to brushes composed of polymers short enough that the height, as measured by the first moment of the density (or h_{para}), scales as D^{-2}. In simulation studies this has been shown to be the case for course-grain brushes up to around 50 monomers in length. Neutron reflectivity studies have shown that the height of polystyrene brushes with molecular weight 330 000 g mol^{-1}, on the order of 3000 monomer units, scales as D^{-2}.[41,54] The influence of the tail region must also be taken into account when considering longer chains. Self-consistent field theory predicts that extent of the tail region will scale as $N^{1/3}$, and the number of monomers in this region will scale as $N^{2/3}$.[42] Thus, the length of the tail relative to the brush height will decrease as N increases, such that the tail will have less influence over the stagnation length of the flow. However, confined geometries exist, such as flow through nano-porous media, where the absolute length of the tail may still have a significant effect on the penetration length.

The point at which the monomers reverse their direction of flow—the flow reversal length, shown in Figure 8—is comparable to the stagnation length, and in most cases it is slightly smaller. It was generally the case that the flow actually penetrated further into the brush than the apparent penetration length determined by fitting the velocity above the brush, such that there was typically a region within the brush at which the liquid was flowing in the direction of shear while the polymer was moving against it.

4.2. Boundary Conditions of Flow over Collapsed Brush in a Poor Solvent. In the poor solvent the polymer brushes collapsed and underwent constrained dewetting from the underlying nonadsorbing substrate, with the exception of the brush with chain separation $D = 2.01\sigma$, which was dense enough to form a stable homogeneous layer. The morphology of the patterns formed—pinned micelles, pancake micelles, and semicontinuous layers, shown in Figure 9—were in line with those previously reported in the literature.[34] The surface coverage of these patterns decreased with increasing chain separation. For the first time we have demonstrated that these collapsed polymer brushes have potential as nanopatterned mixed-slip surfaces, in this case with a slip boundary condition over the polymer-covered regions and no-slip on the exposed substrate. The variation in boundary condition is clearly visible in Figure 12, showing the contrast in liquid velocity above the surface, and the correlation with the underlying morphology of the collapsed brush. These correlations in the velocity dissipated further from the substrate as the flow became more homogeneous, as show in Figure 13. The length over which the flow dissipated is comparable to the lateral length scale of the pattern.

The effective average boundary condition at the collapsed brush is strongly affected by the chain separation, as shown in Figure 15. Our model in eq 8, the open circles in Figure 15, demonstrates that this can be attributed largely to changes in surface coverage and height of the polymer aggregates, both of which decrease with chain separation, as shown in Figure 10. The model qualitatively predicts the decreasing penetration length with chain separation, although overestimates the penetration length. The difference between model prediction and simulation result occurs because the derivation of eq 7 assumes the slip length at any point on the surface is always less than the pattern length scale,[53] while the surfaces in our simulations lie on the borderline of this regime.

Not all polymers will necessarily exhibit a significant slip length in all poor solvents, but the fact that slip length tends to be larger when solid–liquid interactions are weak—as is typically the case for a polymer in a poor solvent—suggests that in a physical experiment it should be possible to identify a polymer chemistry and poor solvent for which a slip boundary condition exists at the polymer–liquid interface.

Polymer brushes capable of forming patterns similar to the ones observed in Figure 9 are relatively simple to prepare by a grafting-to approach.[37] In addition to the potential as valves in nanochannels,[19−21] opening and closing with changes in solvent quality, these surfaces could potentially act as switchable microfluidic mixers,[38] mixing liquids in the collapsed, patterned state, and allowing fluid to pass relatively unperturbed in the swollen state. The challenge here would be to identify a set of polymer, substrate, and fluid chemistries which provide a large contrast in slip length between the liquid–substrate and liquid–polymer interfaces and at the same time having the ability to easily switch the brush between collapsed and swollen conformations.

5. CONCLUSIONS

The relationship between the boundary condition of liquid flow at the interface with a polymer brush and the grafting density of the brush is strikingly different between the good and poor solvent case. In a good solvent the, stagnation length scales as $D^{-2/3}$,as predicted by Alexander and de Genne's scaling analysis, while the height scales as the inverse square of the chain separation, D^{-2}. If the tail region of the density profile is neglected, then the penetration length appears to increase as chains are moved closer together. When the tail region is included in the height, penetration length decreases as chains are moved together for the entire range studied. The freely moving chains in the good solvent undergo a cyclic motion, with the monomers in the region from the top of the brush to approximately the stagnation length moving in the direction of the flow, and the monomer some distance further into the brush moving against it.

The patterns formed during the constrained dewetting of the brush under poor solvent conditions create interesting possibilities for the interaction with fluid flow. For the poor solvent system, increasing the chain separation increases the amount of no-slip substrate exposed and thus results in decreasing overall slip length. While the model we present does not exactly predict the magnitude of the slip length, it captures the general trend of increasing slip length with increasing coverage of polymer on the substrate, as determined by the chain separation.

■ AUTHOR INFORMATION

Corresponding Author

*E-mail: s.hendy@irl.cri.nz (S.C.H.); chiara.neto@sydney.edu.au (C.N.).

Notes

The authors declare no competing financial interest.

■ ACKNOWLEDGMENTS

C.N. and S.C.H. acknowledge the Australian Research Council for funding, and C.N. acknowledges The University of Sydney for funding. This work was supported by an award under the Merit Allocation Scheme on the NCI National Facility at the Australian National University.

■ REFERENCES

(1) Neto, C.; Evans, D. R.; Bonaccurso, E.; Butt, H. J.; Craig, V. S. J. *Rep. Prog. Phys.* **2005**, *68* (12), 2859−2897.
(2) Lauga, E.; Brenner, M.; Stone, H. Microfluidics: The No-Slip Boundary Condition. In *Springer Handbook of Experimental Fluid Mechanics*; Tropea, C., Yarin, A. L., Foss, J. F., Eds.; Springer: New York, 2005; pp 1219−1240.
(3) Bocquet, L.; Barrat, J. L. *Soft Matter* **2007**, *3* (6), 685−693.
(4) Bocquet, L.; Charlaix, E. *Chem. Soc. Rev.* **2010**, *39* (3), 1073−1095.
(5) Uhlmann, P.; Merlitz, H.; Sommer, J.; Stamm, M. *Macromol. Rapid Commun.* **2009**, *30* (9−10), 732−740.
(6) Rau, A. R. P. *J. Biosci.* **2002**, *27* (5), 475−478.
(7) Lauga, E.; Powers, T. R. *Rep. Prog. Phys.* **2009**, *72* (9), 096601.
(8) Choi, K. S.; Yang, X.; Clayton, B. R.; Glover, E. J.; Atlar, M.; Semenov, B. N.; Kulik, V. M. *Proc. Math., Phys. Eng. Sci.* **1997**, *453* (1965), 2229−2240.
(9) Milner, S. T. *Macromolecules* **1991**, *24* (12), 3704−3705.
(10) Brinkman, H. C. *Appl. Sci. Res.* **1947**, *Al*, 27.
(11) Léonforte, F.; et al. *J. Phys.: Condens. Matter* **2011**, *23* (18), 184105.
(12) McLean, S. C.; Lioe, H.; Meagher, L.; Craig, V. S. J.; Gee, M. L. *Langmuir* **2005**, *21* (6), 2199−2208.
(13) Rabin, Y.; Alexander, S. *Europhys. Lett.* **1990**, *13* (1), 49.
(14) Miao, L.; Guo, H.; Zuckermann, M. J. *Macromolecules* **1996**, *29* (6), 2289−2297.
(15) Lai, P. Y.; Binder, K. *J. Chem. Phys.* **1993**, *98* (3), 2366−2375.
(16) Kumaran, V. *Macromolecules* **1993**, *26* (10), 2464−2469.
(17) Clément, F.; Charitat, T.; Johner, A.; Joanny, J. F. *Europhys. Lett.* **2001**, *54* (1), 65.
(18) Müller, M.; Pastorino, C. *Europhys. Lett.* **2008**, *81* (2), 28002.
(19) Adiga, S. P.; Brenner, D. W. *Nano Lett.* **2005**, *5* (12), 2509−2514.
(20) Huang, J.; Wang, Y.; Laradji, M. *Macromolecules* **2006**, *39* (16), 5546−5554.
(21) Dimitrov, D. I.; Klushin, L. I.; Milchev, A.; Binder, K. *Phys. Fluids* **2008**, *20* (9), 092102.
(22) Binder, K.; Kreer, T.; Milchev, A. *Soft Matter* **2011**, *7*, 7159−7172.
(23) Kim, Y. W.; Lobaskin, V.; Gutsche, C.; Kremer, F.; Pincus, P.; Netz, R. R. *Macromolecules* **2009**, *42* (10), 3650−3655.
(24) Pastorino, C.; Binder, K.; Müller, M. *Macromolecules* **2008**, *42* (1), 401−410.
(25) Müller, M.; Pastorino, C.; Servantie, J. *Comput. Phys. Commun.* **2009**, *180* (4), 600−604.
(26) Pastorino, C.; Kreer, T.; Muller, M.; Binder, K. *Phys. Rev. E* **2007**, *76* (2), 026706.
(27) Milchev, A.; Dimitrov, D. I.; Binder, K. *Biomicrofluidics* **2010**, *4* (3), 032202.
(28) Dimitrov, D. I. *J. Chem. Phys.* **2007**, *127* (8), 084905.
(29) Zhou, F.; Huck, W. T. S. *Phys. Chem. Chem. Phys.* **2006**, *8* (33), 3815−3823.
(30) Ouyang, H.; Xia, Z.; Zhe, J. *Microfluid. Nanofluid.* **2010**, *9*, 915−922.
(31) Lim, R. Y. H.; Deng, J. *ACS Nano* **2009**, *3* (10), 2911−2918.
(32) Peleg, O.; Tagliazucchi, M.; Kroeger, M.; Rabin, Y.; Szleifer, I. *ACS Nano* **2011**, *5* (6), 4737−4747.
(33) Lai, P.-Y.; Binder, K. *J. Chem. Phys.* **1992**, *97* (1), 586−595.
(34) Huh, J.; Ahn, C.-H.; Jo, W. H.; Bright, J. N.; Williams, D. R. M. *Macromolecules* **2005**, *38* (7), 2974−2980.
(35) Zhulina, E. B.; Birshtein, T. M.; Priamitsyn, V. A.; Klushin, L. I. *Macromolecules* **1995**, *28* (25), 8612−8620.
(36) Koutsos, V.; van der Vegte, E. W.; Pelletier, E.; Stamouli, A.; Hadziioannou, G. *Macromolecules* **1997**, *30* (16), 4719−4726.
(37) Koutsos, V.; van der Vegte, E. W.; Hadziioannou, G. *Macromolecules* **1999**, *32* (4), 1233−1236.
(38) Hendy, S. C.; Jasperse, M.; Burnell, J. *Phys. Rev. E* **2005**, *72* (1), 016303.
(39) Kremer, K.; Grest, G. S. *J. Chem. Phys.* **1990**, *92* (8), 5057−5086.
(40) Grest, G. S. *Macromolecules* **1994**, *27* (2), 418−426.
(41) Factor, B. J.; Lee, L. T.; Kent, M. S.; Rondelez, F. *Phys. Rev. E* **1993**, *48* (4), R2354−R2357.
(42) Milner, S. T. *J. Chem. Soc., Faraday Trans.* **1990**, *86* (9), 1349−1353.
(43) Kusalik, P. G.; Svishchev, I. M. *Science* **1994**, *265* (5176), 1219−1221.
(44) Milner, S. T. *Science* **1991**, *251* (4996), 905−914.
(45) Charmet, J. C.; de Gennes, P. G. *J. Opt. Soc. Am.* **1983**, *73* (12), 1777−1784.
(46) Milner, S. T.; Witten, T. A.; Cates, M. E. *Europhys. Lett.* **1988**, *5* (5), 413.
(47) Alexander, S. *J. Phys. (Paris)* **1977**, *38* (8), 983−987.
(48) de Gennes, P. G. *Adv. Colloid Interface Sci.* **1987**, *27* (3−4), 189−209.
(49) Ivkov, R.; Butler, P. D.; Satija, S. K.; Fetters, L. J. *Langmuir* **2001**, *17* (10), 2999−3005.
(50) Baker, S. M.; Smith, G. S.; Anastassopoulos, D. L.; Toprakcioglu, C.; Vradis, A. A.; Bucknall, D. G. *Macromolecules* **2000**, *33* (4), 1120−1122.
(51) Milner, S. T.; Witten, T. A.; Cates, M. E. *Macromolecules* **1988**, *21* (8), 2610−2619.
(52) Williams, D. *J. Phys. II* **1993**, *3* (9), 1313−1318.
(53) Hendy, S. C.; Lund, N. J. *Phys. Rev. E* **2007**, *76* (6), 066313.
(54) Kent, M. S.; Lee, L. T.; Factor, B. J.; Rondelez, F.; Smith, G. S. *J. Chem. Phys.* **1995**, *103* (6), 2320−2342.